



Detection of *E. coli* labeled with metal-conjugated antibodies using lateral-flow assay and laser-induced breakdown spectroscopy

Carmen Gondhalekar¹ · Eva Biela² · Bartek Rajwa³ · Euiwon Bae⁴ · Valery Patsekin² · Jennifer Sturgis² · Cole Reynolds¹ · Iyil-Joon Doh⁴ · Prasoon Diwakar⁵ · Larry Stanker⁶ · Vassilia Zorba⁷ · Xianglei Mao⁷ · Richard Russo⁷ · J. Paul Robinson^{1,2}

Received: 24 October 2019 / Accepted: 10 December 2019
© Springer-Verlag GmbH Germany, part of Springer Nature 2020

Abstract

This study explores the adoption of laser-induced breakdown spectroscopy (LIBS) for the analysis of lateral-flow immunoassays (LFIA). Gold (Au) nanoparticles are standard biomolecular labels among LFIA, typically detected via colorimetric means. A wide diversity of lanthanide-complexed polymers (LCPs) are also used as immunoassay labels but are inapt for LFIA due to lab-bound detection instrumentation. This is the first study to show the capability of LIBS to transition LCPs into the realm of LFIA, and one of the few to apply LIBS to biomolecular label detection in complete immunoassays. Initially, an in-house LIBS system was optimized to detect an Au standard through a process of line selection across acquisition delay times, followed by determining limit of detection (LOD). The optimized LIBS system was applied to Au-labeled *Escherichia coli* detection on a commercial LFIA; comparison with colorimetric detection yielded similar LODs (1.03E4 and 8.890E3 CFU/mL respectively). Optimization was repeated with lanthanide standards to determine if they were viable alternatives to Au labels. It was found that europium (Eu) and ytterbium (Yb) may be more favorable biomolecular labels than Au. To test whether Eu-complexed polymers conjugated to antibodies could be used as labels in LFIA, the conjugates were successfully applied to *E. coli* detection in a modified commercial LFIA. The results suggest interesting opportunities for creating highly multiplexed LFIA. Multiplexed, sensitive, portable, and rapid LIBS detection of biomolecules concentrated and labeled on LFIA is highly relevant for applications like food safety, where in-field food contaminant detection is critical.

Keywords Laser-induced breakdown spectroscopy · Lateral-flow immunoassay · Metal-conjugated antibodies · *E. coli* · Lanthanides

✉ J. Paul Robinson
jpr@flowcyt.cyto.purdue.edu

¹ Weldon School of Biomedical Engineering, Purdue University, West Lafayette, IN 47907, USA

² Department of Basic Medical Sciences, Purdue University, West Lafayette, IN 47907, USA

³ Bindley Bioscience Center, Discovery Park, Purdue University, West Lafayette, IN 47907, USA

⁴ School of Mechanical Engineering, Applied Optics Laboratory, Purdue University, West Lafayette, IN 47907, USA

⁵ Mechanical Engineering Department, South Dakota School of Mines & Technology, Rapid City, SD 57701, USA

⁶ United States Department of Agriculture, USDA Research Services, Albany, CA 94706, USA

⁷ Energy Technologies Area, Lawrence Berkeley National Laboratories, Berkeley, CA 94720, USA

Introduction

This paper explores the application of laser-induced breakdown spectroscopy (LIBS) for analysis of standard lateral-flow immunoassay (LFIA) platforms, and LFIA platforms modified with lanthanide biomolecular labels. The combination of these technologies primarily offers advantages for rapid, portable and multiplexed biomolecular detection. Such a detection modality is particularly useful in food inspection and forensics, where rapid in-field identification of food contaminants such as *Escherichia. coli* has wide-spread public health impacts.

LFIA have become popular field-deployable diagnostic tools because they are simple, portable, and low cost [1–3]. LFIA are well described in scientific literature [3, 4]. A common example is the pregnancy test strip, which utilizes gold nanoparticles (GNPs) coated in antibodies for colorimetric

detection of human chorionic gonadotropin hormone. Configurations of LFIA vary greatly, but a common approach is to use a two-step lateral-flow assay design [5]. In this design, an antigen-containing suspension is mixed in a tube with an antigen label. The solution is introduced to one end of a nitrocellulose strip, and capillary forces wick the labeled antigen along the strip. A defined area downstream of the sample introduction zone displays antibodies that immobilize the labeled antigen, but not the background material, which is removed as it continues to travel downstream. The label that is not bound to a target is captured downstream at the control line. The concentrated label at the test and control lines are then detectable, typically through colorimetric means. Similar designs are common in commercial products, many of which have applications in food science, such as bacterial, allergen, and toxin detection [4]. While commercial LFIA are not a stand-alone assessments of analyte presence, ongoing advancements and the advantages of LFIA in portability and cost suggest a promising future, especially for in-the-field detection.

Increasing the sensitivity and quantitative multiplexing capability of LFIA is a key aspect of improving LFIA performance. [2, 4] Multiplexed LFIA for food-contamination detection are uncommon because of sample complexity, limited number of antigen labels (e.g., gold, silver, latex), reagent chemistry on the paper substrate, and spatial design [2]. A common multiplexing approach is to spatially differentiate each antigen across a test cartridge. However, the footprint of the test cartridge increases and becomes more cumbersome as the multiplexing capability increases [2, 3]. An alternative is to use unique labels to differentiate each antigen while maintaining the size of the footprint. This approach would permit a smaller test cartridge design and smaller sample volumes.

Labels typically used among commercial LFIA are gold, silver, and latex beads, which visually contrast the background of the assay substrate and biological matrix by localized surface plasmon resonance [2]. In immunochemistry, fluorochromes are widely used labels because of their specificity and excellent signal-to-noise capacity [6] [7, 8]. However, multiplexing either fluorochromes or gold, silver, or latex particles is challenging for most detection modalities owing to overlapping emission or color profiles, short lifetimes, and background effects [8–11]. These features make it challenging to develop detection modalities that are portable and highly multiplexed.

This study proposes a method to overcome the challenges of multiplexed LFIA by introducing a new detection modality, LIBS—a multi-analyte detection tool [12, 13]. The large number of available labels for LFIA creates opportunities for highly multiplexed assays that can be used as field-deployable or bench-based diagnostic tools. Existing labels that lend themselves to LIBS analysis are polymer-complexed metals,

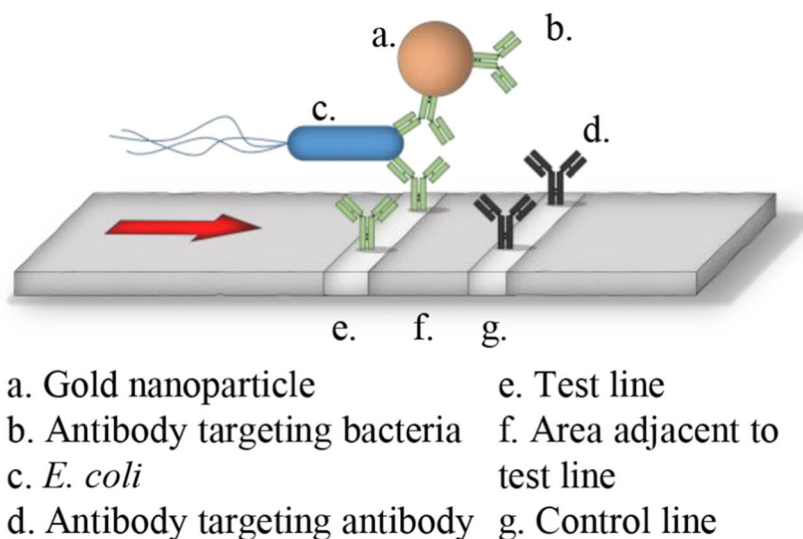
mostly lanthanides (e.g. europium, ytterbium, praseodymium, and neodymium), which have been developed in the last several years for use in immunoassays analyzed by mass cytometry for discoveries primarily in the field of hematology [11, 14]. The diversity of metal labels and the bandwidth of mass cytometry permits highly multiplexed immunoassays [9, 15, 16]. To date, metal-complexed polymers have not been applied to LFIA, possibly because the size, cost, and sample preparation requirements of mass spectrometry precludes their transition into the field of low-cost or portable diagnostics [17]. With the rapid advancements being made in laser and optical sensor technologies, LIBS is becoming increasingly portable [13]. It has potential to become a portable analytical tool for highly multiplexed LFIA that use polymer-complexed metals for antigen labeling.

LIBS is a technique for simultaneous multi-element identification that relies on the generation and spectral analysis of a laser-induced plasma [12]. While it originated as a bench-top instrument, it has recently been developed into a hand-held commercial product, predominantly applied to characterization of soils, rocks, and scrap metal [13, 18]. Significant effort has been undertaken to apply LIBS to biological applications such as microbial identification and toxin detection [13, 19–22]. In a few instances, portable LIBS systems were designed for bio-contaminant detection [19, 23]. Some studies apply LIBS to analysis of clinical samples, where analytes are labeled with metal tags [24–26]. These studies primarily apply gold, iron, titanium, and silicon micro- and nanoparticles as bio-labels detected with LIBS on a porous membrane-like paper.

This is the first study that reports the use of LIBS to detect antigens on a LFIA, and the first to introduce metal-complexed polymers to LFIA. Our approach was LIBS detection of *E. coli* using a gram-negative bacteria detection kit commercialized by Silver Lake Research (Irwindale, CA, USA) for water quality assessment. The kit comprises lyophilized gold nanoparticles that bind to *E. coli* in solution, followed by introduction to a lateral-flow strip that immobilizes the labeled *E. coli* at the detection zone. Conventional analysis of the strip involves visual or image-based analysis of the pink nanoparticles clustered at the test line. We apply and compare image analysis and LIBS.

A bench-based LIBS system was built in-house and optimized for the detection of gold, the label used in the gram-negative bacteria detection kit. A dilution series of *E. coli* was applied to the LFIA and the intensity of the Au signal at the test line vs. adjacent area (Fig. 1) was compared using LIBS and image analysis. Throughout the study, the control line only served as a visual assessment of proper assay function. To determine if metals used for metal-complexed polymer labels would offer more sensitive detection, the LIBS system was also optimized for detection of europium (Eu), neodymium (Nd), praseodymium (Pr), and ytterbium (Yb). LODs for

Fig. 1 Design of a conventional lateral-flow immunoassay. In this example, a suspension of *E. coli* labeled with Au nanoparticles is concentrated at the test line. As the sample continues to flow down the strip, gold nanoparticles also bind to the control line



each lanthanide and Au were then compared. Eu-conjugated antibodies were then used for *E. coli* detection on a modified commercial LFIA.

The results suggest that LOD for Au-labeled *E. coli* detection is comparable between LIBS and image analysis. While Au is the conventional biomolecular label among LFIAs, certain lanthanides like Eu and Yb may be a more favorable alternative when detected with LIBS because they offer lower LODs. A proof of concept study shows that Eu-complexed polymers can be used in a LFIA for labeling *E. coli* followed by LIBS detection, setting the stage for future studies that explore the LOD of microbial detection using this labeling scheme.

In summary, the study suggests ways in which LIBS can be used as a detection modality to improve LFIA sensitivity and multiplexing capability, two aspects deemed important for the success of LFIAs [2, 4]. LFIAs have promise across a wide diversity of fields that require rapid and portable detection of analytes. Enhancing LFIA capabilities using LIBS is particularly relevant to food inspection and forensics, where portability, speed, and accuracy are critical.

Materials and methods

Instrumentation

The LIBS system, described in detail in Gondhalekar et al. 2019 [27], consisted of a 1064-nm 4-ns pulsed laser (Nano SG 150–10, Litron Lasers, Bozeman, MT, USA) with a 150-mJ maximum laser pulse and 10-Hz maximum repetition rate. For experimentation, 35 mJ of pulse energy and a spot size of $\sim 700 \mu\text{m}$ were used. A spectrometer and ICCD from Andor Technologies (SR-500I-B1 and DH320T-18F-E3) were used to measure spectra and control integration time, which was

maintained at 500 ns throughout the study. Ablations took place in a chamber fitted with a vacuum pump and air filter to remove hazardous aerosols. Pressure inside the chamber was maintained at 1 atm. The chamber was supported by a XYZ stage (TPA0348B-00, The Precision Alliance, Fort Mill, SC, USA) that permitted pre-programmed and automated movement of samples. Coupling the timing between laser pulses (10 Hz) and automated stage movement allowed for rapid sampling.

Peak identification

Peaks for Au, Eu, Nd, Pr, and Yb were identified by first acquiring a high-resolution (0.1 nm) broad spectrum (200–600 nm) for 2 μg of each metal on nitrocellulose. Each metal is originally in an oxidized form dissolved in 2% HNO_3 or 5% HCl at a stock concentration of 1000 mg/L (05779-100ML, 39,956, 41,695, 59,947, and 38,168, Sigma Aldrich, St. Louis, MO, USA). Ten microliters of 200 mg/L solutions for each metal were added to $6 \times 6 \text{ mm}$ nitrocellulose squares and dried. While some studies use spectrographs that cover a broad spectral range, the system used here collected a relatively narrow ($\sim 30 \text{ nm}$) range. Therefore, to obtain the 200–600 nm spectra, multiple 30 nm increments of the spectrum were acquired and then stitched together. Each increment consisted of an average of 25 shots, one shot per location on the square (one square per 25 shots). The process was repeated for delay times 0.5, 1, 2, 3, and 4 μs . Integration time was 500 ns for all treatments. Emission lines from the metals of interest were cross-checked using the NIST Atomic Spectra Database [28]. Three peaks per metal element were selected to determine LOD based on the following criteria: high intensity (after signal standardization), low interference with nitrocellulose background, and positive match to the NIST database [28].

Limit of detection of other metals

LOD was determined for Au, Eu, Yb, Nd, and Pr at the wavelengths and delay times determined in the peak identification portion of the study (Table 1). Au, Eu, Yb, and Nd standards were diluted to 100, 50, 25, 12.5, 6.25, and 3.125 mg/L using either 2% HNO₃ or 5% HCl as the diluent. For Pr, the concentrations 369, 290, 230, 183, 145, and 115 mg/mL were used. Ten microliters of each dilution step was added to 6 × 6 mm nitrocellulose squares and dried. As a negative control, 10 μL of 2% HNO₃ or 5% HCl was added to nitrocellulose squares. Each treatment consisted of 3 replicates/squares. Each nitrocellulose square was shot 25 times, 1 shot per location.

LOD values are reported as ppm, defined as milligrams of metal per kilogram of nitrocellulose. The average weight of nitrocellulose per 6 × 6 mm laser-cut section was 1 mg.

Gold-nanoparticle paper-based assay preparation and testing

WaterSafe® bacteria test strips (Silver Lake Research, Azusa, CA, USA) use Au to label gram-negative bacteria like *E. coli*. While the strips are typically interpreted visually or with image analysis, we attempt to compare this modality to a LIBS system optimized for gold detection.

A colony of *E. coli* K12 was selected from a tryptic soy agar culture plate and suspended in phosphate-buffered saline (PBS), from which a dilution series was prepared. The number of colony-forming units (CFU)/mL of the stock was determined by plating the last 4 dilution steps and colony counting after a 24-h incubation period at 37 °C. One hundred

microliters of *E. coli* suspensions with a concentration of 3.50E6, 3.50E5, 1.75E5, 3.51E4, 7.35E3, 4.23E3, 9.43E2, 0 CFU/mL were mixed with 100 μL of gold nanoparticles from WaterSafe® Bacterial test kits suspended in purified water (optical density (OD) = 0.4) for 5 min. WaterSafe® Bacterial test strips from the kit were introduced to the solutions (3 replicates per dilution) for 10 min. A pink color at the control line developed on each strip, indicating that the assay was functioning properly. A pink coloration at the test lines was also observed to form; the intensity of the pink line decreased with decreasing *E. coli* concentration.

The nitrocellulose portion of the test strip was separated from the conjugate and waste pad, and air-dried for 2 h. The membranes were then imaged using a stereomicroscope. Images were then used for analysis.

LIBS was performed after imaging. The parameters determined to be optimal for Au detection were applied to LIBS detection of Au-labeled *E. coli* on a LFIA. Of the three wavelengths identified for Au, 242.795 nm and 267.595 nm lines were selected because they had the best LODs and fit within the same 30 nm acquisition window. The test line and area adjacent to the test line were each shot 6 times in 6 locations per strip.

Europium-complexed polymer and gold-nanoparticle paper-based assay preparation and testing

While Au nanoparticle labels are common among LFIA, an exploratory study was performed to determine whether lanthanide-complexed polymers conjugated to antibodies could be used as an alternative.

Table 1 Element emission lines listed in order of smallest to greatest LOD. LOD data were acquired from a dilution series, whose slope, y-intercept, SNR of the first dilution step, and R² values and delay time are listed in the table

Element	Ionization	Emission line	Delay (us)	SNR at maximum concentration	R ²	Slope	Y-intercept	LOD(ppm)
Eu	II	420.504	2.000	499.208	0.976	0.640	1.476	1.052
Yb	II	369.419	0.500	622.379	0.986	0.746	1.338	1.577
Yb	II	328.937	0.500	1512.346	0.959	0.519	2.179	1.684
Eu	II	412.973	2.000	434.058	0.976	0.604	1.485	3.200
Eu	II	397.197	3.000	235.437	0.981	0.648	1.131	15.309
Au	I	242.795	0.500	180.703	0.992	0.807	0.683	15.968
Au	I	267.595	0.500	266.706	0.995	0.570	1.302	34.371
Nd	II	401.224	2.000	75.952	0.991	0.828	0.238	152.826
Yb	II	265.375	0.500	216.096	0.988	0.997	0.247	168.742
Nd	II	406.108	3.000	56.504	0.980	0.791	0.209	205.522
Au	I	312.295	0.500	32.993	0.957	1.701	-1.755	528.340
Pr	II	411.846	3.000	70.971	0.977	0.316	-22.707	1528.197
Pr	II	440.882	3.000	60.910	0.974	0.194	-8.295	1766.937
Pr	II	414.311	3.000	92.022	0.973	0.230	-14.041	2145.206
Nd	II	430.777	3.000	24.583	0.542	0.132	1.037	NA

A total of 120 μL of an *E. coli* stock solution (OD 0.014, roughly 5×10^7 CFU/mL) was mixed with gold nanoparticles from the Watersafe® kit (OD 0.4). After a 5-min incubation, 30 μL of 0.5 mg/mL anti-mouse antibody conjugated to Eu-complexed polymers using Fluidigm's metal conjugation kit (Fluidigm, 201151A, San Francisco, CA) were added to the solution. After a 1-h incubation, 150 μL of the mixture was introduced to the WaterSafe® test strip for 10 min. The nitrocellulose portion of the test strip was separated from the conjugate and waste pad, and air-dried for 2 h. Two types of negative controls were used: the first underwent the same treatment as the experimental group, but 120 μL PBS was used instead of 120 μL *E. coli* suspension; the second type of negative control was treated similarly to the experimental group, except that 30 μL PBS was used instead of 30 μL anti-mouse antibody conjugated to Eu.

For LIBS detection of the Eu-labeled *E. coli* on the strip, the parameters determined to be optimal for Eu emission detection (Table 1) were applied. The test line and area adjacent to the control line were each shot 8 times in 8 locations per strip.

Data analysis

LIBS spectra were analyzed using a custom-developed procedure written in R language for statistical computing [29]. A sliding median filter estimated the background across the wavelength range and was subtracted from the raw data. To determine signal-to-noise ratio (SNR), the data were then standardized by dividing by the standard deviation of the noise, estimated using a second median filter. This process was repeated for every spectrum acquired with LIBS.

Limit of detection was determined by applying the following formula to a dilution series of the metal standard:

$$LOD = ((3.3 * SD_0 + \mu_0) - b) / m$$

Where SD_0 is the standard deviation of the SNR in the area adjacent to the test line, μ_0 is the mean SNR of the emission line in the negative control, b is the y -intercept of the regression line, and m is the slope of the regression line. The regression line equation was derived from a linear fit of the SNR vs. concentration data for each analyte. To obtain a linear fit for the lanthanide dilution series, both axes were log-transformed. To obtain a linear fit for the *E. coli* dilution series, only SNR was log-transformed.

Image analysis of WaterSafe® strips utilized ImageJ [30] to first perform background subtraction followed by image inversion. "Background" was considered the area adjacent to the test line in the treatment with 0 CFU/mL *E. coli*. Integrated density, or the product of area and mean gray value, was determined for each test line and area adjacent to the test line.

Results

Peak identification and limit of detection for Au, Eu, Nd, Yb, and Pr

A high-resolution 200–600 nm spectrum was acquired for Au, Eu, Nd, Pr, and Yb standards on nitrocellulose at different delay times to identify strong emission lines. Figure 2 displays the

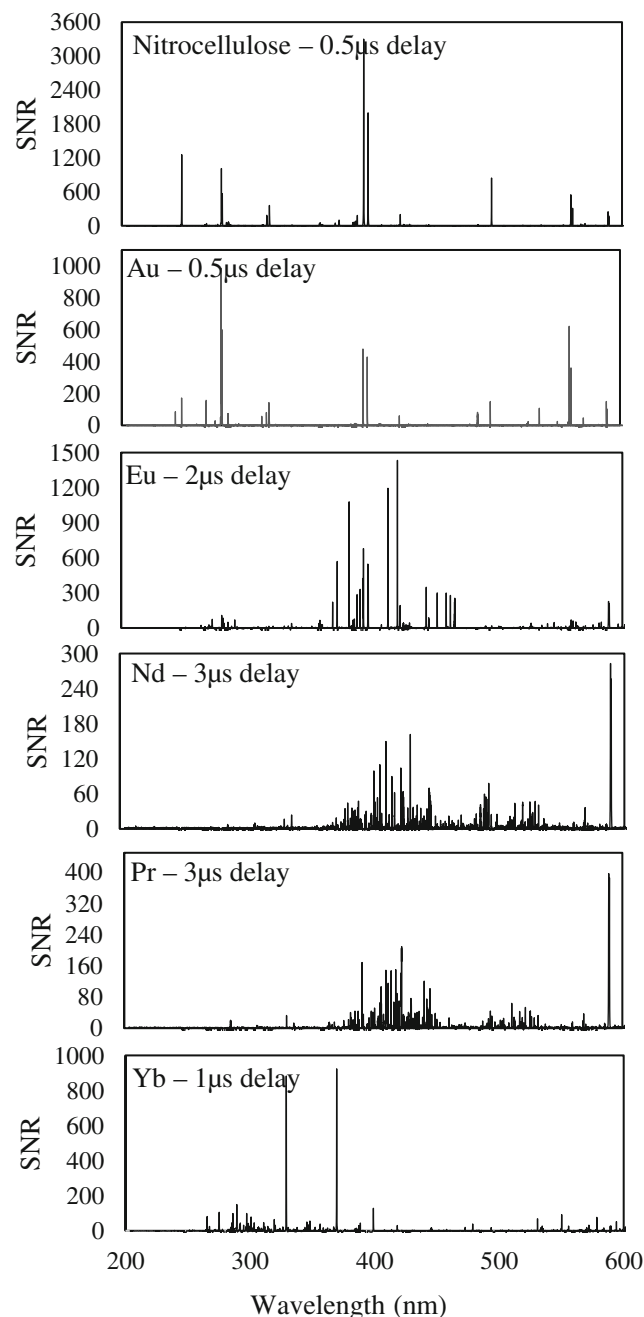


Fig. 2 From top to bottom are the 200–600 nm spectra of nitrocellulose (background), followed by the background-subtracted spectra of Au, Eu, Nd, Pr, and Yb standards. Au, Eu, and Yb display intense, low-density emission lines. Nd and Pr display weaker high-density emission lines

high-resolution spectra and the negative control. Data for Au, Eu, and Yb show these elements to have a few low-density, intense emission lines. On the other hand, Nd and Pr have multiple high-density, low-SNR emission lines. The results matched the atomic emission lines reported by the NIST database [28]. Each emission line was observed to have a delay time at which it was most intense. While Au and Yb tended to have strong emission lines early in plasma formation (0.5- and 1- μ s delay), other elements tended to peak later (Fig. 3). Optimum delay times for select emission lines for each element are summarized in Table 1. The line selection was based on high SNR, low interference with the nitrocellulose background, and close proximity to other element lines. Overall, the Eu line at 420.504 nm had the greatest SNR at a delay of 2 μ s, followed by Yb 269.44 nm at 1 μ s, Au 267.639 nm at 0.5 μ s, Nd 430.271 nm at 3 μ s, and Pr

411.846 nm. Three selected emission lines per metal (listed in Table 1) and their corresponding delay times were used to determine the LOD of each metal.

The measured LODs (Table 1) were compared to determine which metal would be the best candidate as a biomolecular label in a LFIA analyzed with LIBS. A positive non-linear relationship was observed between metal concentration and SNR for the selected lines for each metal. A log transformation of both SNR and concentration yielded a linear fit between $R^2 = 0.96$ and 0.99 for all emission lines except Nd 430.77 nm (Table 1). Nd 430.77 nm did not show a linear relationship potentially attributed to the interfering line originating from the nitrocellulose. The slope of the relationship between SNR and log-transformed concentration (ppm) depended on the emission line—Yb 265.375 nm had the greatest rate of decrease, Nd

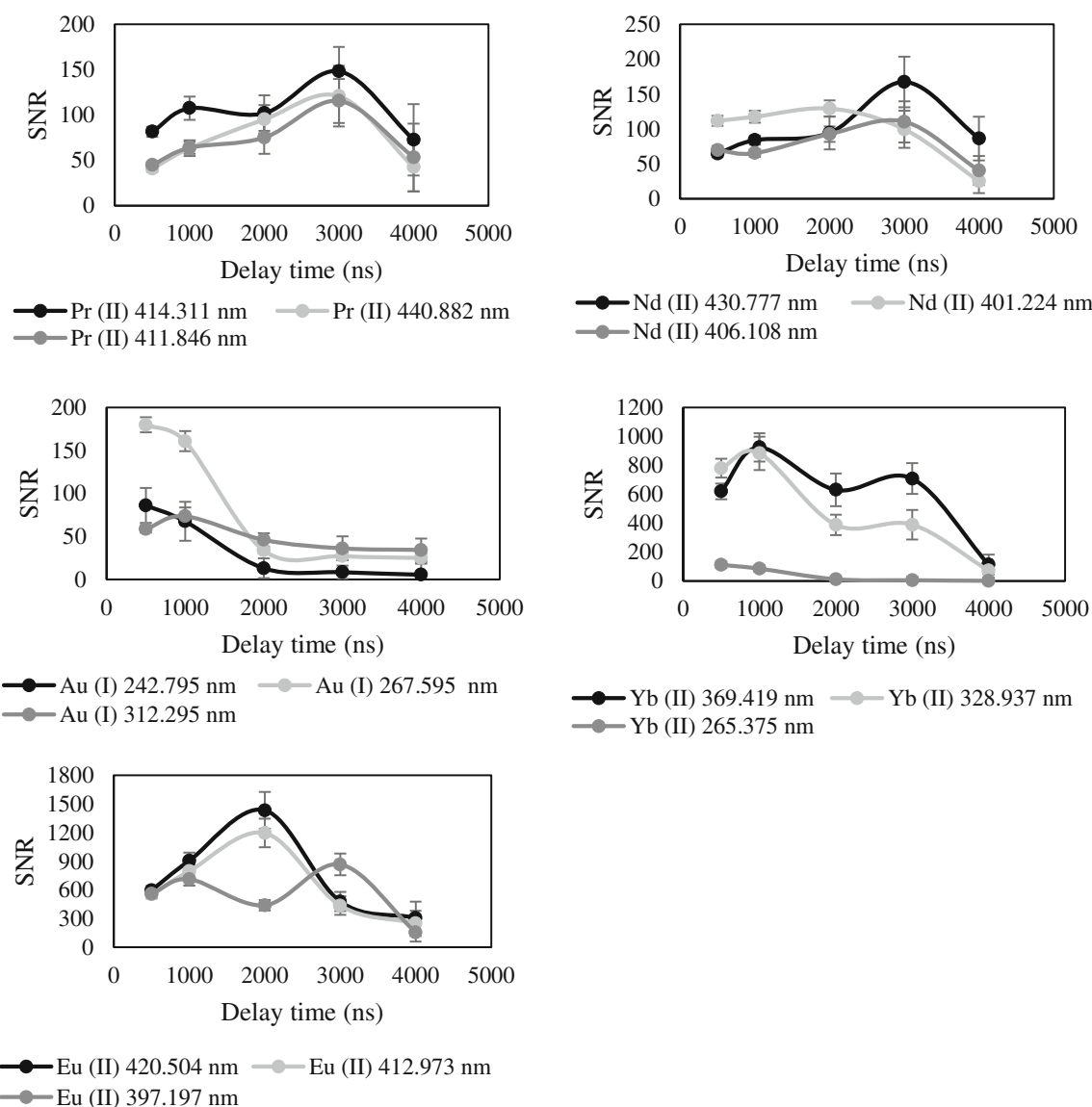


Fig. 3 Response in SNR upon changing delay in acquisition time for Au, Eu, Nd, Pr, and Yb standards on nitrocellulose. Each line is observed to peak at specific delay times. The delay time that yielded the highest SNR was used to acquire LOD data

430.777 nm the least (Table 1). SNR vs. concentration for each line is represented in Fig. 4. The Eu 420.504-nm line offered the best LOD at 1.05 ppm. For Au, the best emission line was found to be 242.795 nm with an LOD of 15.97 ppm. LODs for other metals and their select lines can be found in Table 1.

E. coli detection using gold nanoparticles: LIBS vs. image analysis

WaterSafe® detection strips use gold nanoparticles to label gram-negative bacteria, in this case *E. coli*. The LOD of

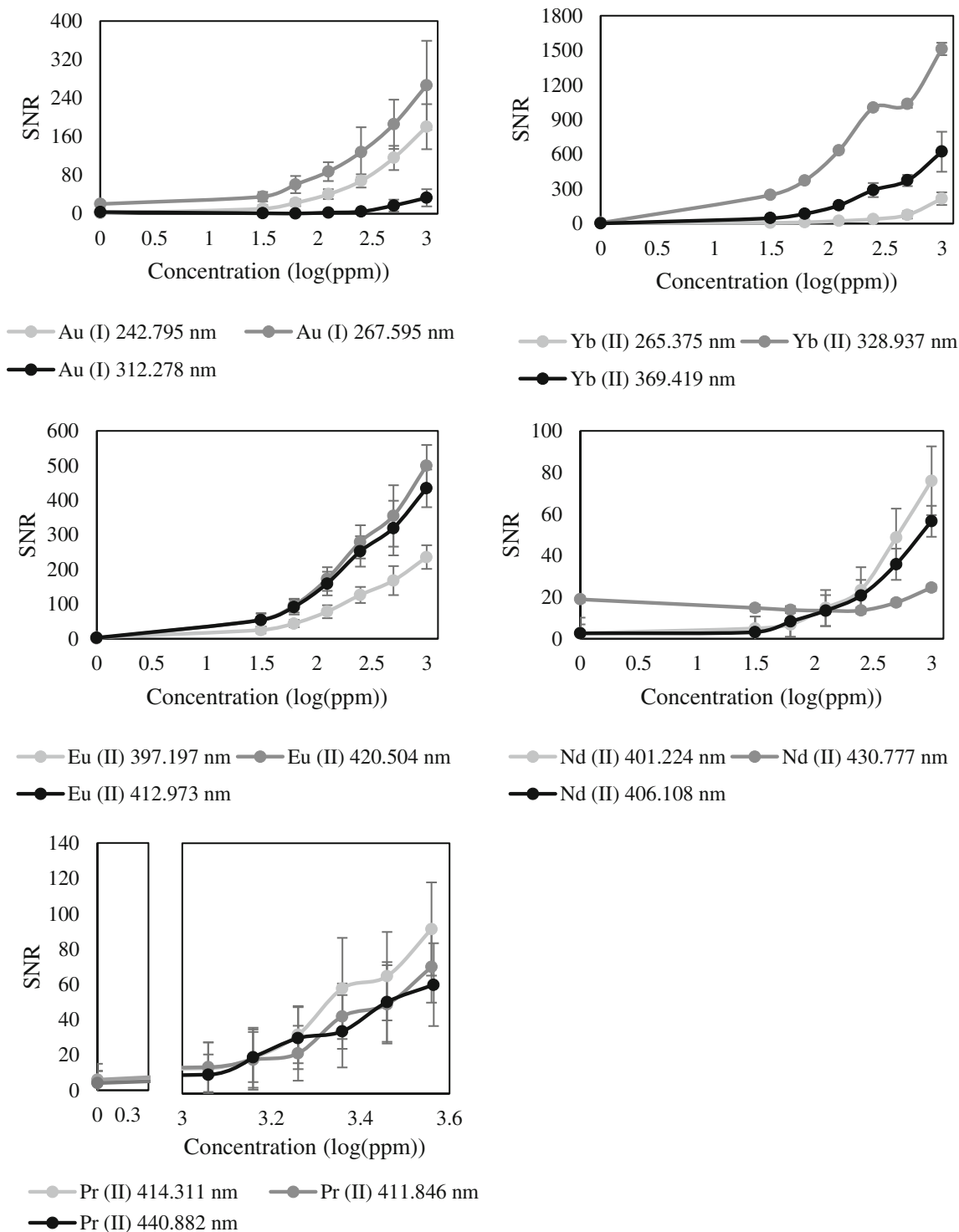


Fig. 4 Dilution series of Au, Eu, Nd, Pr, and Yb standards on nitrocellulose. Response in SNR of three selected lines per metal were used to find the LIBS system LOD for the metal

colorimetric detection was compared to that of LIBS detection of Au. Image analysis of the diagnostic strips showed a positive linear relationship between integrated density and log-transformed *E. coli* concentration ($R^2 = 0.99$). LOD using image analysis was determined to be $8.890E3$ CFU/mL. LIBS analysis of the Au 242.795 nm line also showed a positive linear relationship but with a worse linear fit ($R^2 = 0.93$). LOD using LIBS was $1.03E4$ CFU/mL, comparable to that of image analysis.

E. coli detection using Eu-complexed polymers

The standard protocol for WaterSafe® detection strips was modified to use Eu-complexed polymers to label *E. coli*.

The treatment containing *E. coli* and Eu-complexed antibodies (experimental treatment) displayed a Eu signal 63 times stronger at the test line compared to the area adjacent to the test line ($P < 0.0001$; 95% CI 30.40 to 44.10), indicating the presence of *E. coli*. The difference is similar between the test line of the experimental treatment and areas adjacent to the test line in the negative controls.

In the negative control treatment where Eu-labels are absent (*E. coli* is present), there is little to no difference in Eu signal between the test lines and adjacent areas ($P = 0.1317$; 95% CI -0.85 to 5.85). In the negative control treatment where *E. coli* is absent (Eu label is present), there is some difference in Eu signal between the test lines and adjacent areas ($P = 0.4815$, 95% CI -6.634 to 3.29). This difference may be attributed to a low degree of residual or nonspecifically bound Eu-labeled antibody at the test line (Fig. 5).

Discussion

Au is a transition metal with many applications in electronics, jewelry, medicine, and biomolecular detection. LIBS publications on Au detection primarily address the mining industry [31, 32] and analysis of ores, but also the jewelry trade [33], archeology [34], and detection of biomolecules with gold labels [26]. Au nanoparticles are often used for conjugation to biomolecules owing to their stability and chemical surface properties. These properties make them excellent for use in paper immunoassays, where biomolecules can be detected based on the pink coloration of Au nanoparticles. While LFAs are analyzed primarily with imaging, our goal in this study was to explore LIBS as a potentially portable, more sensitive, and multiplexed alternative.

While the LIBS LOD for Au reported in the literature is 0.8–2.6 ppm in ores, few if any studies refer to the LOD of Au on nitrocellulose paper [26]. Since many LFAs use nitrocellulose paper as a platform on which to concentrate and label analytes, it is important to determine the optimal parameters for gold detection on this material. After optimization, we

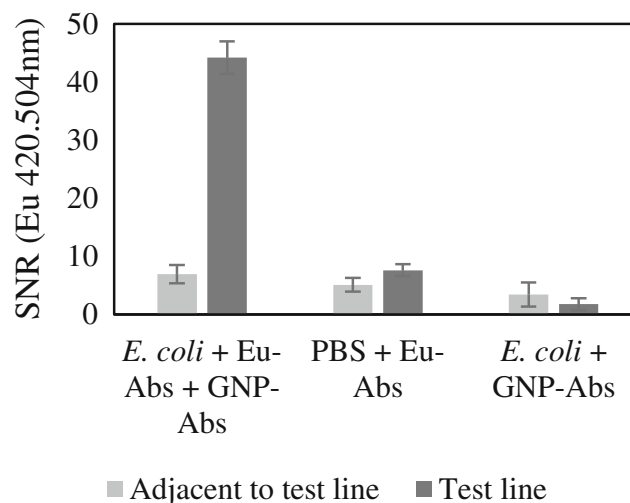


Fig. 5 LIBS analysis of the test line (light gray) and area adjacent to the test line (dark gray) of a lateral-flow assay for gram-negative bacteria detection. Three treatments are displayed: the experimental sample consisting of *E. coli* labeled with Eu-conjugated antibodies (Eu-Abs) and gold-nanoparticle-conjugated antibodies (GNP-Abs); a negative control consisting of Eu-Abs and GNP-Abs, but no *E. coli*; and a second negative control consisting of *E. coli* and GNP-Abs but not Eu-conjugated antibodies. The Eu signal was highest in the test line for the treatment consisting of *E. coli* and Eu-conjugated antibodies. The adjacent area in this treatment showed significantly lower Eu signal, indicating that labeled *E. coli* was aggregated at the test line

achieve a limit of detection of 16.0 ppm. This serves as a benchmark for comparing other metal labels to determine which offers the best LOD.

A LIBS system with low LOD is particularly important when attempting to detect rare analytes. Food contaminants can be extremely hazardous even in minute quantities, and therefore detection modalities must be sensitive and fast. *E. coli* is a common food and water contaminant, and acceptable concentrations of *E. coli* in drinking water and food vary according to strain. As an example, for generic *E. coli* detection, the U.S. Department of Agriculture states that chicken rinsate containing ≥ 1000 CFU/mL during industrial processing is unacceptable. [35] Concentrations below this value are considered either acceptable or marginally acceptable.

The present study utilized WaterSafe® Bacteria Detection strips to detect gram-negative bacteria, in this case *E. coli*, using Au labels. The LOD reported by the manufacturer for these strips is 1000 CFU/mL, enough to potentially distinguish between acceptable and unacceptable concentrations of *E. coli* in chicken rinsate. Strips were introduced to a dilution series of *E. coli*. As with many LFAs that use gold, latex, or silver labels, the results were assessed by detecting the label at the detection zone with image analysis. LOD with image analysis was found to be $8.890E3$ CFU/mL, on the same order as the manufacturer's reported LOD. To determine if LIBS could achieve a better LOD, the pink detection zones were analyzed for the presence of Au using an optimized system. The resulting LOD was comparable to image analysis ($1.03E4$

CFU/mL). There is significant potential for improving LIBS limit of *E. coli* detection by using a label that produces a more intense signal than Au. Lanthanides are good candidates because they are already widely used in the field of immunochemistry for antigen labeling.

Literature regarding detection of lanthanides with LIBS often refers to the area of nuclear fuel quality assessment and industrial waste, given their importance in uranium extraction and as magnets for commercial electronics [36]. LIBS publications on lanthanides were not found to refer to their use as biomolecular labels [37] despite their extensive use in biomedical sciences and immunoassays. In LIBS articles that refer to detection of the lanthanides Pr, Yb, Eu, and Nd, the matrices and instrument parameters such as laser energy and wavelength, diffraction grating, and detector vary significantly [38, 39]. The variation among these factors led the authors of those studies to choose, out of the many emissions produced by lanthanides, those that will yield the best LOD. To select appropriate emission lines for this study, the 200–600 nm spectrum of five lanthanides on paper were collected at different delay times. While Eu, Au, and Yb had simple spectra, Nd and Pr had many closely spaced emission lines. The literature suggests similar findings of certain lanthanides having multiple high-density emission lines [40]. Two or three intense lines that had high SNR, little interference with the nitrocellulose background, and in proximity of other lines belonging to the same element were selected for further examination at their optimal delay time. Reported LIBS detection limits for Eu are 1–209 ppm, Nd 11–500 ppm, Pr 3–40 ppm, and Yb 1–156 ppm, depending on the material, acquisition parameters, and data analysis approach [38, 41–44]. We find that our best LODs were 1.1, 1.5, 152.8, and 1528.2 ppm for Eu, Yb, Nd, and Pr respectively. The data show that different emission lines for the same metal have different rates of decay across the dilution series, indicating that the most intense emission line at high concentrations does not necessarily mean the best LOD.

When comparing the LOD of lanthanides to gold, it is found that Eu and Yb have LODs 10 orders of magnitude less than Au. Therefore, LFAs analyzed with LIBS may be able to achieve more sensitive detection of the bio-analyte when it is labeled with Eu and Yb rather than the same quantity of Au.

While many LIBS studies involving lanthanide detection use standards applied to substrates such as paper, this study goes further by demonstrating the practical application of a lanthanide label for microbial detection. We demonstrated *E. coli* labeled with Eu and captured on a lateral-flow device was clearly detectable with LIBS. While this proof-of-concept experiment shows great potential in the combined use of LIBS, LFAs, and lanthanide labels, a large body of work is needed to compare the LOD of different labels and to compare LIBS to conventional analytical methods. Future work also involves determining if different labels can be simultaneously

detected on the same test line. Doing so would permit detection of multiple types of microbial food contaminants in a single test line.

While the potential for multi-analyte detection on a single test strip without compromising assay footprint is promising, application to in-field detection also requires a portable LIBS system. While the LIBS system used in this study is bench-based, future work involves applying the optimized parameters for detection of Au, Eu, Yb, Pr, and Nd to a handheld device.

Conclusion

This study introduces LIBS as a functional and innovative detection modality for biomolecules concentrated and labeled on LFAs. It is the first to explore LIBS as an approach for making LFAs more sensitive and multiplexed. Like LFAs, LIBS can also be designed as a portable unit, making the pairing of these two technologies applicable to rapid in-field detection of biomolecules. While current and future work focuses on designing this system for food-contamination detection, the function of this tool can expand to detection of chemical and biological warfare agents.

Acknowledgments The authors would like to acknowledge the Laser Technologies Group at Lawrence Berkeley National Laboratories and the Environmental Microbial & Food Safety Laboratory: Beltsville, MD. This research was partially supported by the US Department of Energy, Office of Defense Nuclear Nonproliferation Research and Development, under contract number DE-AC02-05CH11231 at the Lawrence Berkeley National Laboratory. We thank Dr. Gary Nolan's group at Stanford University and the United States Department of Agriculture for their assistance in antibody conjugation chemistry. We also acknowledge support from the National Science Foundation (DGE-1333468) and funding from the U.S. Department of Agriculture, project 1935-42000-072-02G, Center for Food Safety Engineering at Purdue University.

Compliance with ethical standards

Conflict of interest The authors declare that they have no conflict of interest.

References

1. Zhao W, Ali MM, Aguirre SD, Brook MA, Li Y. Paper-based bioassays using gold nanoparticle colorimetric probes. *Anal Chem*. 2008;80(22):8431–7. <https://doi.org/10.1021/ac801008q>.
2. Liana DD, Raguse B, Gooding JJ, Chow E. Recent advances in paper-based sensors. *Sensors (Basel)*. 2012;12(9):11505–26. <https://doi.org/10.3390/s120911505>.
3. Bahadır EB, Sezginürk MK. Lateral flow assays: principles, designs and labels. *TrAC Trends in Anal Chem*. 2016;82:286–306. <https://doi.org/10.1016/j.jim.2014.10.010>.
4. Posthuma-Trumpie GA, Korf J, van Amerongen A. Lateral flow (immuno)assay: its strengths, weaknesses, opportunities and

- threats. A literature survey. *Anal Bioanal Chem.* 2009;393(2):569–82. <https://doi.org/10.1007/s00216-008-2287-2>.
5. Wild DG. 7.3.1 pregnancy tests. *Immunoassay handbook - theory and applications of ligand binding, ELISA and related techniques* (4th edition). Elsevier. .
 6. Giepmans BNG, Adams SR, Ellisman MH, Tsien RY. The fluorescent toolbox for assessing protein location and function. *Science.* 2006;312(5771):217.
 7. Zhang J, Li B, Zhang L, Jiang H. An optical sensor for Cu(II) detection with upconverting luminescent nanoparticles as an excitation source. *Chem Comm.* 2012;48(40):4860–2. <https://doi.org/10.1039/C2CC31642K>.
 8. Xu S, Dong B, Zhou D, Yin Z, Cui S, Xu W, et al. Paper-based upconversion fluorescence resonance energy transfer biosensor for sensitive detection of multiple cancer biomarkers. *Sci Rep.* 2016;6: 23406. <https://doi.org/10.1038/srep23406>.
 9. Yao Y, Liu R, Shin MS, Trentalange M, Allore H, Nassar A, et al. CyTOF supports efficient detection of immune cell subsets from small samples. *J Immunol Methods.* 2014;415:1–5. <https://doi.org/10.1016/j.jim.2014.10.010>.
 10. Resch-Genger U, Grabolle M, Cavaliere-Jaricot S, Nitschke R, Nann T. Quantum dots versus organic dyes as fluorescent labels. *Nat Methods.* 2008;5:763. <https://doi.org/10.1038/nmeth.1248>.
 11. Kanje S, Herrmann AJ, Hober S, Mueller L. Next generation of labeling reagents for quantitative and multiplexing immunoassays by the use of LA-ICP-MS. *Analyst.* 2016;141(23):6374–80. <https://doi.org/10.1039/C6AN01878E>.
 12. Cremers DA. *Handbook of laser-induced breakdown spectroscopy.* Chichester, West Sussex, England: John Wiley & Sons; 2006.
 13. Rakovský J, Čermák P, Musset O, Veis P. A review of the development of portable laser induced breakdown spectroscopy and its applications. *Spectrochim Acta Part B: Atomic Spectroscopy.* 2014;101:269–87. <https://doi.org/10.1016/j.sab.2014.09.015>.
 14. Majonis D, Herrera I, Ornaty O, Schulze M, Lou X, Soleimani M, et al. Synthesis of a functional metal-chelating polymer and steps toward quantitative mass cytometry bioassays. *Anal Chem.* 2010;82(21):8961–9. <https://doi.org/10.1021/ac101901x>.
 15. Yang JY, Herold DA. Chapter 13 - Evolving platforms for clinical mass spectrometry A2 - Nair, Hari. In: Clarke W, editor. *Mass spectrometry for the clinical laboratory.* San Diego: Academic Press; 2017. p. 261–276.
 16. Tanner SD, Baranov VI, Ornaty OI, Bandura DR, George TC. An introduction to mass cytometry: fundamentals and applications. *Cancer Immunol Immunotherapy.* 2013;62(5):955–65. <https://doi.org/10.1007/s00262-013-1416-8>.
 17. Maher S, Jjunju FPM, Taylor S. Colloquium: 100 years of mass spectrometry: perspectives and future trends.(Report). 2015;87(1): 113–130. doi:<https://doi.org/10.1103/RevModPhys.87.113>.
 18. Galbács G. A critical review of recent progress in analytical laser-induced breakdown spectroscopy. *Anal Bioanal Chem.* 2015;407(25):7537–62. <https://doi.org/10.1007/s00216-015-8855-3>.
 19. Gottfried JL, De Lucia FC, Munson CA, Miziolek AW. Standoff detection of chemical and biological threats using laser-induced breakdown spectroscopy. *Appl Spectrosc.* 2008;62(4):353–63. <https://doi.org/10.1366/000370208784046759>.
 20. Barnett C, Bell C, Vig K, Akpovo AC, Johnson L, Pillai S, et al. Development of a LIBS assay for the detection of Salmonella enterica serovar Typhimurium from food. *Anal Bioanal Chem.* 2011;400(10):3323–30. <https://doi.org/10.1007/s00216-011-4844-3>.
 21. Rehse S, Miziolek A. Recent advances in the use of laser-induced breakdown spectroscopy (LIBS) as a rapid point-of-care pathogen diagnostic. *Proceedings of SPIE - The International Society for Optical Engineering.* 2012;8371:1. <https://doi.org/10.1117/12.919256>.
 22. Samuels AC, DeLucia FC, McNesby KL, Miziolek AW. Laser-induced breakdown spectroscopy of bacterial spores, molds, pollens, and protein: initial studies of discrimination potential. *Appl Opt.* 2003;42(30):6205–9. <https://doi.org/10.1364/AO.42.006205>.
 23. Modlitbova P, Farka Z, Pastucha M, Porizka P, Novotny K, Skladal P, et al. Laser-induced breakdown spectroscopy as a novel readout method for nanoparticle-based immunoassays. *Mikrochim Acta.* 2019;186(9):629. <https://doi.org/10.1007/s00604-019-3742-9>.
 24. Jr FC, Samuels A, Harmon R, Walters R, McNesby K, LaPointe A, et al. Laser-induced breakdown spectroscopy (LIBS): a promising versatile chemical sensor technology for hazardous material detection. *Sensors Journal, IEEE.* 2005;5:681–9. <https://doi.org/10.1109/JSEN.2005.848151>.
 25. Markushin Y, Sivakumar P, Connolly D, Melikechi N. Tag-femtosecond laser-induced breakdown spectroscopy for the sensitive detection of cancer antigen 125 in blood plasma. *Anal Bioanal Chem.* 2015;407(7):1849–55. <https://doi.org/10.1007/s00216-014-8433-0>.
 26. Markushin Y, Melikechi N, O. AM, Rock S, Henderson E, Connolly D, editors. *LIBS-based multi-element coded assay for ovarian cancer application.* SPIE BiOS; 2009: SPIE.
 27. Yuri Markushin NM. Sensitive detection of epithelial ovarian cancer biomarkers using tag-laser induced breakdown spectroscopy. InTech: *Ovarian Cancer*; 2012.
 28. Gondhalekar C, Rajwa B, Bae E, Patsekina V, Sturgis J, Kim H, Doh I-J, Diwakar P, Robinson JP. Multiplexed detection of lanthanides using laser-induced breakdown spectroscopy: a survey of data analysis techniques. 2019. p. 1101609–9.
 29. Kramida A, Ralchenko Y, Reader J, Team NA. NIST Atomic Spectra Database (version 5.6.1). <http://physics.nist.gov/asd3>. Accessed 5/3/2017.
 30. Team R. RStudio: integrated development environment for R. Boston, MA: RStudio, Inc.
 31. Schneider CA, Rasband WS, Eliceiri KW. NIH image to ImageJ: 25 years of image analysis. *Nat Methods.* 2012;9(7):671–5.
 32. Diaz D, Hahn DW, Molina A. Quantification of gold and silver in minerals by laser-induced breakdown spectroscopy. *Spectrochim Acta Part B: Atomic Spectroscopy.* 2017;136:106–15. <https://doi.org/10.1016/j.sab.2017.08.008>.
 33. Ahmed N, Ahmed R, Baig M. Analytical analysis of different karats of gold using laser induced breakdown spectroscopy (LIBS) and laser ablation time of flight mass spectrometer (LA-TOF-MS). *Plasma Chem Plasma Process.* 2018;38(1):207–22. <https://doi.org/10.1007/s11090-017-9862-2>.
 34. Jurado-López A, De Castro MDL. Chemometric approach to laser-induced breakdown analysis of gold alloys. *Appl Spectrosc.* 2003;57(3):349–52. <https://doi.org/10.1366/000370203321558281>.
 35. Abdelhamid M, Grassini S, Angelini E, Ingo GM, Harith MA. Depth profiling of coated metallic artifacts adopting laser-induced breakdown spectrometry. *Spectrochim Acta Part B: Atomic Spectroscopy.* 2010;65(8):695–701. <https://doi.org/10.1016/j.sab.2010.03.017>.
 36. FSIS. 9CFR Part 304 Federal Register Rules and Regulations. In: *Agriculture, editor.: Office of the Federal Register, National Archives and Records Administration*; 1996. p. 38563–9037.
 37. Martin MZ, Fox RV, Miziolek AW, Jr, André N. Spectral analysis of rare earth elements using laser-induced breakdown spectroscopy. *SPIE Sensing Technology + Applications.* SPIE: FCD; 2015.
 38. Balaram V. Rare earth elements: a review of applications, occurrence, exploration, analysis, recycling, and environmental impact. *Geosci Front.* 2019;10(4):1285–303. <https://doi.org/10.1016/j.gsf.2018.12.005>.
 39. Alamelu D, Sarkar A, Aggarwal SK. Laser-induced breakdown spectroscopy for simultaneous determination of Sm, Eu and Gd in

- aqueous solution. *Talanta*. 2008;77(1):256–61. <https://doi.org/10.1016/j.talanta.2008.06.021>.
40. Ishizuka T. Laser emission spectrography of rare earth elements. *Anal Chem*. 1973;45(3):538–41. <https://doi.org/10.1021/ac60325a024>.
 41. Martin M, Martin RC, Allman S, Brice D, Wymore A, Andre N. Quantification of rare earth elements using laser-induced breakdown spectroscopy. *Spectrochim Acta Part B: Atomic Spectroscopy*. 2015;114(C):65–73. <https://doi.org/10.1016/j.sab.2015.10.005>.
 42. Bhatt CR, Jain JC, Goueguel CL, McIntyre DL, Singh JP. Measurement of Eu and Yb in aqueous solutions by underwater laser induced breakdown spectroscopy. *Spectrochim Acta B At Spectrosc*. 2017;137(C):8–12. <https://doi.org/10.1016/j.sab.2017.09.009>.
 43. Hartzler DA, Bhatt CR, Jain JC, McIntyre DL. Evaluating laser-induced breakdown spectroscopy sensor technology for rapid source characterization of rare earth elements. *J Energy Res Technol*. 2019;141(7). <https://doi.org/10.1115/1.4042747>.
 44. Yang X, Hao Z, Shen M, Yi R, Li J, Yu H, et al. Simultaneous determination of La, Ce, Pr, and Nd elements in aqueous solution using surface-enhanced laser-induced breakdown spectroscopy. *Talanta*. 2017;163:127–31. <https://doi.org/10.1016/j.talanta.2016.10.094>.

Publisher's note Springer Nature remains neutral with regard to jurisdictional claims in published maps and institutional affiliations.